1   # Adaptive pathways of coral populations on the Great Barrier Reef
2
3   Mikhail V. Matz[1*], Eric A. Treml[2], Galina V. Aglyamova[1], Madeleine J. H. van Oppen[2,3]
4   and Line K. Bay[3]
5
6   [1] Department of Integrative Biology, University of Texas at Austin, 205 W 24th St. C0990,
7   Austin, Texas 78712, USA
8   [2] School of BioSciences, University of Melbourne, Victoria 3010 Australia
9   [3] Australian Institute of Marine Science, QLD, Australia
10
11   * Author for correspondence, matz@utexas.edu
12

13   **Abstract**
14   Reef-building corals are extremely important for maintenance of marine biodiversity and coastal
15   economy and are currently under severe threat from anthropogenic warming. Warming is
16   predicted to drive preferential survival of warm-adapted genotypes that have migrated to cooler
17   locations and result in an overall decline in genetic diversity due to bleaching-related mortality.
18   To quantify these trends, we analyzed five populations of a common coral *Acropora millepora*
19   along the latitudinal extent of the Great Barrier Reef (GBR). Population genomic analysis
20   revealed that most populations were demographically distinct and that migration was indeed
21   preferential southward, from lower (warmer) to higher (cooler) latitudes. However, no recent
22   increase in southward migration was detectable, and inferred migration rates remained closely
23   correlated with predictions of a biophysical model of larval dispersal based on ocean currents.
24   There was also no evidence of recent declines in genetic diversity. A multi-locus adaptation
25   model indicated that standing genetic variation spread across latitudes could be sufficient to fuel
26   continuous adaptation of *A. millepora* metapopulation to warming over the next 100-200 years.
27   Unexpectedly, we found that naturally low heritability of thermal tolerance in reef-building corals
28   due to contribution from horizontally transmitted algal symbionts would facilitate longer
29   metpopulation persistence. Still, despite good prospects for gradual adaptation, our model
30   predicted increase in severity of mortality events due to random thermal anomalies, which could
31   lead to much faster coral extinction if there are ecological feedbacks preventing rapid reef
32   recovery.
33

34   **Significance statement**: Can long-lived organisms such as reef-building corals adapt fast enough
35   to keep up with the historically unprecedented rate of sea surface warming? Here we combine
36   population genomics, biophysical modeling, and evolutionary simulations to argue that
37   populations of a common reef-building coral (*Acropora millepora*) spread across latitudes on the
38   Great Barrier Reef could harbor sufficient genetic variation to fuel efficient adaptation to
39   increasing temperature for another century and perhaps longer. However, corals will be
40   increasingly more sensitive to extreme heat waves despite ongoing adaptation to gradual
41   warming, which could precipitate their extinction much sooner. Our study underscores the key

42   role of standing genetic variation in the future persistence of coral reefs and calls for novel reef
43   management strategies to facilitate natural adaptation process.
44
45   Hot water coral bleaching, caused by global warming, is devastating coral reefs around the world
46   (*1*) but there is room for hope if corals can adapt to increasing temperatures (*2*). Many coral
47   species have wide distributions that span environments that differ dramatically in their thermal
48   regimes, demonstrating that efficient thermal adaptation has occurred in the past (*3*). But can
49   coral adaptation keep up with the unprecedentedly rapid current rate of global warming (*4*)? One
50   way for corals to achieve rapid thermal adaptation is through genetic rescue, involving the spread
51   of existing heat tolerance alleles from low-latitude, warm-adapted populations to higher-latitude,
52   warming regions, via larval migration (*5*, *6*). We have previously demonstrated the presence of
53   genetic variants conferring high thermal tolerance in a low-latitude *A. millepora* population (*5*). It
54   can be expected that global warming will cause preferential survival of warm-adapted poleward
55   migrants because they will be following their thermal optimum, whereas individuals migrating in
56   the opposite direction would find themselves in increasingly mismatched environments (Fig. 1 A,
57   B). Another likely population-level effect of recent declines in coral cover (*7*) is a reduction in
58   overall genetic diversity, potentially limiting both the scope and the rate of adaptation.
59
60   Here, we test these predictions in *Acropora millepora*, a common reef-building coral from the
61   most ecologically prominent and diverse coral genus in the Indo-Pacific (staghorn corals,
62   *Acropora*). We have analyzed genome-wide genetic variation using 2bRAD (*8*) in five
63   populations of *A. millepora* along the latitudinal range of the GBR (Fig. 1 A). We genotyped 18-
64   28 individuals per population at >98% accuracy and with a >95% genotyping rate. Analysis of
65   population structure based on ~11,500 biallelic SNPs separated by at least by 2,500 bases agreed
66   with previous microsatellites results (*9*, *10*), and revealed very low levels of genetic divergence,
67   with only the Keppel Islands population being potentially different from the others (Fig. 1 D and
68   Fig. S1). We observed increasing genetic divergence with geographical distance ("isolation by
69   distance", Fig. 1 C) that supports population divergence, however, pairwise F_{ST} were small and
70   did not exceed 0.014 even between the southernmost and northernmost populations (Keppel and
71   Wilkie). To gain a deeper insight into coral demography, we used Diffusion Approximation for
72   Demographic Inference (*dadi,* (*11*)) to more rigorously test for population subdivision and infer
73   pairwise migration rates among populations and population sizes. *dadi* is a coalescent-based
74   method that optimizes parameters of a pre-specified demographic model to maximize the
75   likelihood of generating the observed allele frequency spectrum (for two populations it is
76   essentially a two-dimensional histogram of allele frequencies, Fig. S2). Being a likelihood-based
77   method, *dadi* can be used to compare alternative models using likelihood ratio tests and Akaike
78   Information Criterion (AIC).
79
80   We used AIC to confirm that our populations are separate demographic units. For each pair of
81   populations we generated 120 bootstrapped datasets by resampling genomic contigs and
82   performed delta-AIC comparison of two demographic models, a split-with-migration model and a
83   no-split model (Fig. S3 B). The split-with-migration model assumed two populations that have

84 split some time *T* in the past, potentially have different sizes *N1* and *N2*, and exchange migrants
85 at different rates (*m12* and *m21*) depending on direction. The no-split model allowed for ancestral
86 population size to change at time *T* but not for a population split, so the experimental data were
87 modeled as two random samples from the same population of size *N*. The majority of bootstrap
88 replicates (88-100%) showed AIC advantage of the split-with-migration model for all but one
89 pair of populations (Sudbury-Magnetic, 39% bootstrap support; Fig. S3). This indicates that the
90 populations are demographically distinct despite very low F_{ST}. This result highlights the power of
91 coalescent analysis relative to classical approaches (such as F_{ST}) that assume genetic equilibrium,
92 i.e., that populations have been stable for thousands of generations.
93
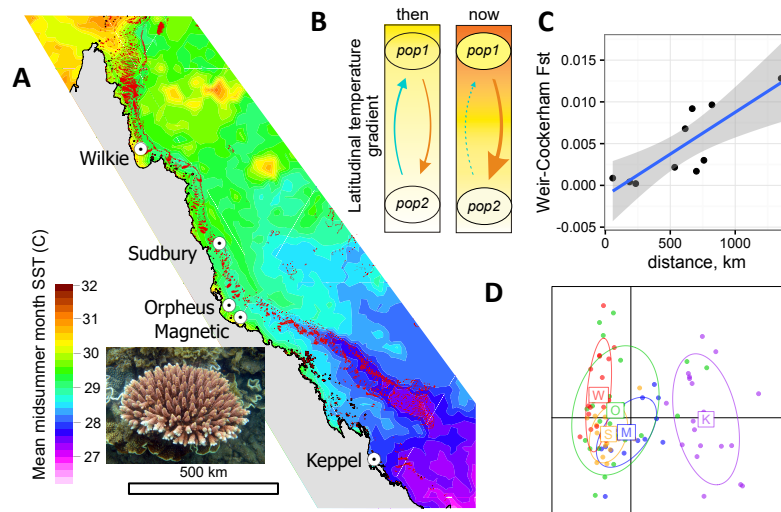
94
95 Figure 1. The population setting and background for our study. (A) Locations of sampled populations
96 where mean midsummer month sea surface temperature differed by up to ~3°C. Inset: *Acropora millepora*.
97 (B) Working hypothesis under global warming: Warm-adapted low-latitude genotypes that migrate to
98 higher latitudes would be following their physiological optimum and hence expected to survive better than
99 migrants in the opposite direction. (C) Increase of pairwise F_{ST} with distance, both indicating weak genetic
100 divergence along the GBR, and (D) principal component analysis of genome-wide genetic variation. On
101 panel D, centroid labels are initial letters of population names as in panel A.
102

103 We then determined pairwise migration rates from the split-with-migration model and estimated
104 their confidence limits from bootstrap replicates. For all pairwise analyses except Wilkie-Sudbury
105 migration in southward direction exceeded northward migration, and this difference was
106 significant in seven out of nine cases (Fig. 2 A and Fig. S3A). Linear mixed model analysis of
107 direction dependent mean migration rates with a random effect of destination (to account for
108 variation in total migration rate) confirmed the overall significance of this southward trend
109 (P_{MCMC} <1e-4).
110

111 It is important to note that our pairwise migration rates captured the cumulative effect of genetic
112 exchange between populations, which included direct migration and the spread of alleles via other

3

113   stepping-stone populations. Such rates do not directly reflect the numbers of larvae exchanged
114   between populations but are very informative in the genetic rescue context. They represent the
115   per-generation rate of replacement of the destination population genotypes by genotypes from the
116   source population, which is essentially the rate at which genetic rescue could proceed.
117
118   To investigate whether the southward migration bias was due to higher survival of southward
119   migrants relative to northward migrants, as predicted under global warming (Fig. 1 B), we
120   developed a biophysical model of coral larval dispersal on the Great Barrier Reef. This model
121   quantified the per-generation migration potential among coral reef habitat patches in the GBR
122   based on ocean currents and parameters of larval biology (*12*, *13*). We found that the genetic and
123   biophysical migration rates were very closely correlated (Mantel test: r = 0.79, P= 0.008, Fig. 2
124   C).
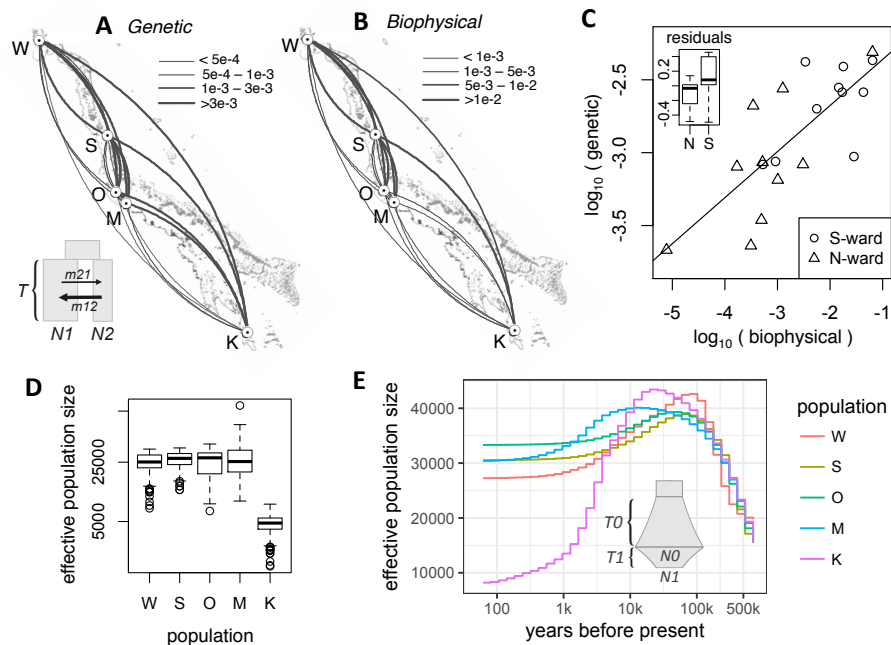
125
126
127   Figure 2. Demography of *A. millepora* populations on the GBR. (A) Arc-plot of migration rates among
128   populations reconstructed from population genetic data. Inset: *dadi* model used: ancestral population splits
129   into two populations of unequal sizes (N1 and N2) some time T in the past, these populations exchange
130   migrants at different rates depending on direction. (B) Migration rates according to the biophysical model.
131   On panels A and B, the arcs should be read clockwise to tell the direction of migration; line thickness is
132   proportional to the migration rate. (C) Correlation between log-transformed biophysical and genetic
133   migration rates (Mantel r = 0.79, P = 0.008). Inset: box-plot of residuals from the linear regression.
134   Southward migration tends to exceed northward migration even after accounting for predictions of the
135   biophysical model (P =0.058), suggesting higher survival of southward migrants. (D) Box plot of effective
136   population sizes inferred by the split-with-migration model (panel A) across all population pairs and
137   bootstrap replicates. (E) Historical changes in effective population sizes inferred using a single-population
138   *dadi* model with two periods of exponential growth (*T0* and *T1*, reaching sizes *N0* and *N1*, inset), averaged
139   across bootstrap replicates.

4

140   Although the biophysical model explained most of the southward migration bias in the genetic
141   data, the residuals were still in favor of southward migration (Fig. 2 C, inset; P = 0.058).
142   While this residual excess suggest preferential survival of southward migrants, as predicted by
143   our hypothesis (Fig. 1 B). These genetic predictions represent historical averages since the
144   populations split and did not resolve any potential recent migration changes.

145

146   To determine any recent changes in southward migration, we evaluated a similar basic split-with-
147   migration model (Fig. 2A) that allowed for a change in migration over the past 75-100 years. The
148   new model suggested some recent migration changes, but there was no consistent change between
149   northward and southward migration (Fig. S4). Delta-AIC bootstrap analysis favored the new
150   model over the basic one only for two pairs of populations, Wilkie-Orpheus and Wilkie-Magnetic
151   (85 and 60% bootstrap support, respectively). We conclude that with the current data and analysis
152   techniques we cannot yet detect the effect of recent warming on preferential direction of coral
153   migration along the GBR.

154

155   The GBR has already warmed by 0.8ºC since the end of last century (*14*) and may have already
156   reduced genetic diversity in *A.millepora* populations. We used *dadi* to infer effective population
157   sizes, which is a measure of genetic diversity and one of the key parameters determining the
158   population's adaptive potential (*15*). The results of the split-with-migration model (Fig. 2 A)
159   were consistent for all population pairs and indicated that Keppel population was about one-fifth
160   the size of others (Fig. 2 D, E). This result was not surprising since the Keppel population
161   frequently suffers high mortality due to environmental disturbances and was therefore is expected
162   to show diminished long-term effective population size (*9*). We also used a single-population
163   *dadi* model that allowed for two consecutive growth/decline periods (Fig. 2 E, inset) to
164   reconstruct effective sizes of individual populations through time (Fig. 2 E and Fig S5). All
165   populations showed evidence of growth prior to the last glaciation, 500-20 thousand years ago
166   (Fig 2 E), which aligned well with the fossil record of rising dominance of *Acropora* corals on
167   Indo-Pacific reefs during this period (*16*). It has been suggested that the fast growth and early
168   sexual maturation of *Acropora* corals gave them an advantage relative to most other reef-building
169   corals during dynamic changes in the reef-forming zone due to the sea level changes
170   accompanying glacial cycles (*16*). Our results suggest that *A. millepora* populations have been in
171   stasis or slow decline since sea level changes abated (Fig. S5), although the inclusion of an
172   additional growth/decline period only improved the model fit significantly for the Keppel
173   population (Fig S6). None of the populations showed evidence of accelerated decline in effective
174   population size over the past few hundred years. Although our samples were collected in the
175   early-mid 2000s, our results are still relevant since they characterize populations only two-three
176   coral generations ago. Disturbances that have affected corals since then would not yet have
177   substantially impacted genetic diversity.

178

179   To evaluate whether standing genetic variation contributed by local thermal adaptation could
180   sustain evolution of the *A. millepora* metapopulation in response to warming, we have developed
181   a multi-QTL model of metapopulation adaptation in SLiM (*17*). The model was parameterized

182   with population sizes and migration rates inferred from the genetic analysis (Fig. 2 A, D), and
183   with differences in midsummer monthly mean temperature among populations (Fig. 1 A). The
184   number of QTLs and their effect sizes, phenotypic plasticity (standard deviation of the Gaussian
185   slope of fitness decline when phenotype mismatches the environment) and heritability (proportion
186   of phenotypic variation attributable to genetics) can all be varied in the model. It can also
187   incorporate climate scenarios with any combination of directional, cyclical and random changes.
188   The model also allows for new mutations but here the new mutation rate was set to zero. This was
189   to assess the contribution of only the standing genetic variation that was introduced into
190   populations at the start of simulation as random QTL effects. The climate scenario started with a
191   pre-adaptation to local thermal conditions for 2,000 generations. Assuming a generation time of
192   of 5 years in *A. millepora* (*18*) this corresponded to the period of stable temperature since the last
193   deglaciation. After pre-adaptation, the temperature was increased at a rate of 0.05^{o}C/generation in
194   all populations, corresponding to the projected 0.1^{o}C warming per decade (*19*). Throughout the
195   simulation temperature was allowed to fluctuate randomly between generations to approximate El
196   Nino Southern Oscillation (ENSO): the temperature deviations were drawn from a normal
197   distribution with a standard deviation of 0.25^{o}C. The size of populations was kept constant
198   throughout the pre-adaptation period and scaled linearly with the populations' relative fitness
199   (mean current fitness divided by the mean fitness at the end of pre-adaptation period) during
200   warming. Migration rates from a population also scaled linearly with the population's fitness. In
201   this way, a population declining in fitness would shrink in size and stop contributing migrants to
202   other populations.
203
204   Our model suggested that, with only ten thermal QTLs, under all combinations of heritability and
205   plasticity the pre-adapted metapopulation would be able to persist through the warming for at
206   least 50-100 generations and, in some realistic cases, much longer (Fig. 3 and Figs. S7-S8).
207   Migration in general and southward migration in particular substantially contributed to this
208   persistence (Fig. 3 E, F), underscoring the importance of the spread of warm-adapted genotypes
209   from lower to higher latitudes (*5*).
210
211   Predictably, higher phenotypic plasticity promoted population persistence and stability against
212   random thermal anomalies, but we were rather surprised to observe a similar positive effect of
213   lower heritability, set to the values observed in coral quantitative genetics experiments (0.25-0.5,
214   (*17*); Fig 3, Fig. S7). One specific reason why corals are expected to show low heritability of
215   thermal tolerance is that much of natural variation in this trait in corals is due to the type of algal
216   symbionts (*Symbiodinium* spp. (*20*)). Photo-symbionts are not transmitted from parent to
217   offspring in the majority of coral species (*21*), and although host genetics can have some effect on
218   the choice of *Symbiodinium* in the next generation (*22*) environment has a very strong effect on
219   this association (*20, 23*). Higher persistence under low heritability and high plasticity is most
220   likely explained by the fact that they both allow for higher standing genetic variation to be
221   retained in populations (Fig. S9). During warming, this variation lasts longer as a source of
222   adaptive genetic variants, enabling up to 5°C increase in mean thermal tolerance over 150
223   generation (Fig. 3 G and Fig. S7). Higher plasticity partially rescued the drop in fitness due to low

6

224   heritability (Fig. 3 B and D, Fig. S7). Another notable tendency observed with all parameter
225   settings was that during warming the fitness (and hence the size) of adapting populations began to
226   fluctuate following random thermal anomalies, and the amplitude of these fitness fluctuations
227   increased as the warming progressed even though the amplitude of thermal anomalies did not
228   change (Fig. 3 H). These fluctuations correspond to severe mortality events induced by thermal
229   extremes due to ENSO and affected warm-adapted populations most, which very much resembles
230   the situation currently observed throughout the world (1).
231
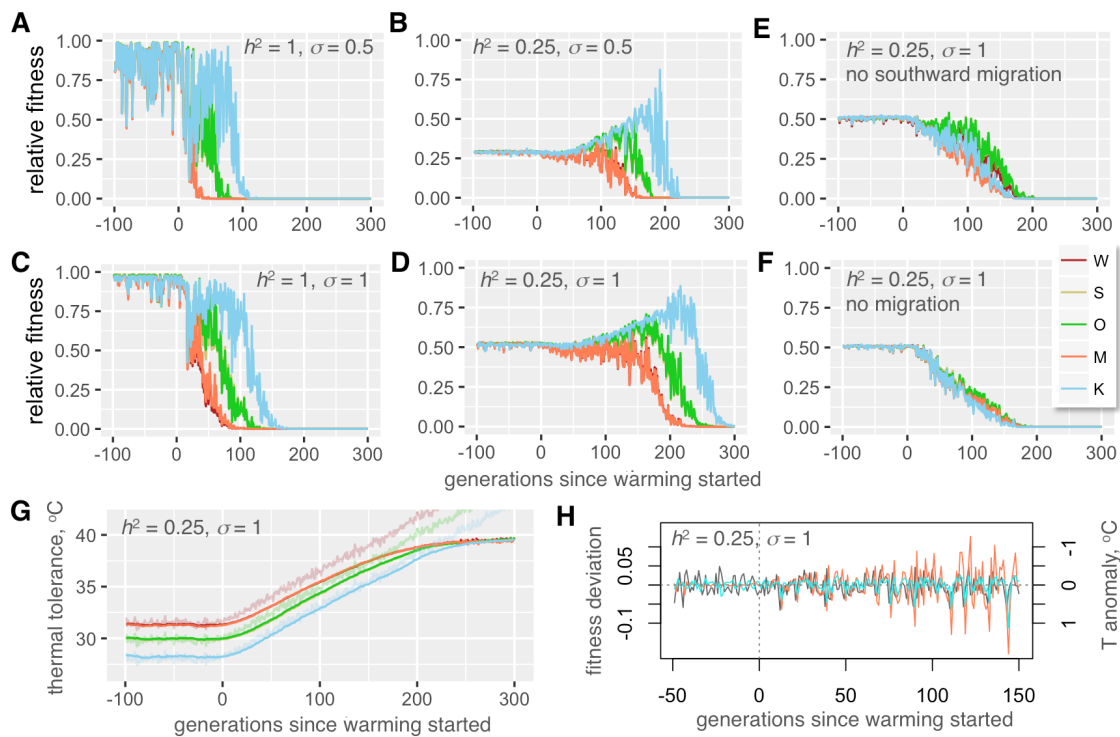
232
233   Figure 3. Modeling coral metapopulation persistence under global warming. (A-D) Fitness of modeled
234   populations depending on heritability of thermal tolerance (h^2, proportion of tolerance variation explained
235   by genetics), phenotypic plasticity (σ, standard deviation of the Gaussian slope of fitness decline away from
236   the phenotypic optimum, in degrees C), and presence-absence of migration (E, F). On panels A-F, y-axis is
237   observed fitness relative to maximal fitness at the genetically determined optimum, averaged over all
238   individuals in a population. Warm-adapted populations (W and M) are shown as red-tint traces, populations
239   from mild thermal regime (S and O) are green-tint traces, and the cool-adapted population (K) is the blue
240   trace. Note nearly complete overlap between traces for pairs of populations pre-adapted to the same
241   temperature (W,M and S,O). (G) Thermal tolerances of evolving populations. Thin noisy lines are modeled
242   temperatures at different locations. (H) Modeled random temperature anomalies (grey line) and fluctuations
243   in populations' fitness (the colored lines are residuals from loess regression over fitness traces on panel D;
244   Wilkie: orange line, Keppel: blue line). Note the inverse sign of temperature anomalies: this more clearly
245   shows the correspondence between rise in temperature and drop in fitness in the next generation. As
246   warming progresses, populations (especially originally warm-adapted ones) become increasingly sensitive
247   to random temperature fluctuations.
248

7

249   There are several uncertainties in our model associated with coral biology. Higher number of
250   QTLs and/or their larger effect sizes would promote higher genetic variation and lead to longer
251   population persistence. To keep the analysis conservative, our model included only ten QTLs,
252   which is likely much fewer that the actual number of thermal QTLs in acroporid corals (*20*). We
253   also kept the distribution of QTL effect sizes narrow: with the current settings and ten QTLs, at
254   the start of simulation only about 2% of corals deviated from the mean thermal tolerance by more
255   than 1.5^{o}C in either direction. Such narrow variation makes adaptation to the thermal gradient of
256   ~3°C along the GBR non-trivial, but still, at present there is no experimental data to evaluate
257   whether even such narrow variation is realistic. Our model was also conservative in using
258   effective population sizes suggested by genetic analysis as census sizes. In highly fecund marine
259   organisms census sizes tend to substantially exceed effective population sizes, sometimes by
260   orders of magnitude (*24*), which would strongly promote higher genetic diversity and population
261   persistence. Moreover, we modeled only our five populations rather than the whole GBR, which
262   would have resulted in much higher standing genetic variation in the metapopulation, promoting
263   longer persistence.

264

265   As for phenotypic plasticity, in simulations shown on Fig. 3, $\sigma = 0.5$ and $\sigma = 1$ corresponded to
266   86% and 40% decline in fitness if the individual's phenotype mismatched the environment by
267   1°C. The existing data on the issue of coral thermal plasticity are somewhat conflicting. One
268   study shows that acroporid corals can successfully acclimatize to environments differing in
269   maximum temperatures by as much as 2°C (*25*); however, another study found that coral grew
270   52-80% more slowly when transplanted among locations differing by 1.5^{o}C average temperature,
271   (*26*). Although it is not possible to directly place these results into our quantitative plasticity
272   framework, the former study supports the higher plasticity setting ($\sigma = 1$) while the latter study
273   supports $\sigma = 0.5$. It must also be noted that both these studies involved *in situ* transplantations and
274   hence the effect of temperature remains confounded with other local fitness-affecting
275   environmental parameters. Also, in adult corals plasticity is likely lower that in larvae and
276   recruits, which are expected to exhibit non-reversible developmental plasticity associated with
277   metamorphosis and establishment within a novel environment (*27*). Future experiments that
278   expose multiple genetically distinct coral individuals to a range of temperatures under controlled
279   laboratory settings are required to rigorously quantify variation in thermal optima and plasticity in
280   natural populations.

281

282   In conclusion, we found that genetic diversity and migration patterns of our study species were
283   not yet affected by global warming and were well positioned to facilitate persistence of the GBR
284   metapopulation for a century or more. However, despite ongoing adaptation to gradual
285   temperature increase, corals will become increasingly more sensitive to local thermal anomalies,
286   especially among the originally warm-adapted populations. The 10-85% mortality in the Northern
287   GBR as a result of 2016 bleaching event (*28*) could be a particularly sobering recent
288   manifestation of this trend. Our model assumed that recovery from such mortality events would
289   depend solely on the demographic exchange between coral populations. However, ecological
290   feedbacks such as shifts to an alternative ecological stable state (*29*) might substantially decrease

291　the rate of reseeding and recovery of affected reefs. In that case, the increase in severity of
292　bleaching-related mortality might lead to much faster coral extinction than predicted by our
293　model.
294
295　More research into phenotypic plasticity and genetic variation in coral thermal tolerance and its
296　genetic architecture (number of QTLs and their effect sizes) is needed to further improve the
297　predictive power of our model. The estimated migration in the order of 10 - 100 migrants per
298　generation could be feasibly facilitated by assisted gene flow efforts (*30*) without risking
299　disruption of the natural local adaptation patterns (*31*). Corals are declining on reef world-wide
300　and there is an urgent need to develop new solutions to effectively manage the impacts of global
301　processes such as climate change at local management scales. The broad characterization of
302　genetic diversity, local thermal adaptation and migration pathways in multiple reef-building coral
303　species would greatly inform both traditional spatial management and novel assisted gene flow
304　approaches and should therefore be given high priority.
305
306　**Methods**
307
308　*Genotyping*
309
310　This study relied predominantly on samples described by van Oppen et al (*10*), with addition of
311　several samples from Orpheus and Keppel islands that were used in the reciprocal transplantation
312　experiment described by Dixon et al (*32*). The samples were genotyped using 2bRAD (*8*)
313　modified for Illumina sequencing platform; the latest laboratory and bioinformatics protocols are
314　available at https://github.com/z0on/2bRAD_GATK. BcgI restriction enzyme was used and the
315　samples retained for this analysis had 2.3-20.2 (median: 7.45) million reads after trimming and
316　quality filtering (no duplicate removal was yet implemented in this 2bRAD version). The reads
317　were mapped to the genome of the outgroup species, *Acropora digitifera* (*33, 34*), to polarize the
318　allelic states into ancestral (as in *A. digitifera*) and derived, e.g., (*35, 36*). Genotypes were called
319　using GATK pipeline (*37*).
320
321　Preliminary analysis of sample relatedness using vcftools (*38*) revealed that our samples included
322　several clones: four repeats of the same genotype from the Keppel Island (van Oppen et al (*10*)
323　samples K210, K212, K213 and K216), another duplicated genotype from Keppel (samples K211
324　and K219), and one duplicated genotype from Magnetic Island (samples M16 and M17). All
325　other samples were unrelated. We took advantage of these clonal replicates to extract SNPs that
326　were genotyped with 100% reproducibility across replicates and, in addition, appeared as
327　heterozygotes in at least two replicate pairs (script replicatesMatch.pl with hetPairs=2 option).
328　These 7,904 SNPs were used as "true" SNP dataset to train the error model to recalibrate variant
329　quality scores at the last stage of the GATK pipeline. During recalibration, we used the transition-
330　transversion (Ts/Tv) ratio of 1.438 determined from the "true" SNPs to assess the number of false
331　positives at each filtering threshold (as it is expected that an increase of false positive calls would
332　decrease the Ts/Tv ratio towards unity). We chose the 95% tranche, with novel Ts/Tv = 1.451.

9

333   After quality filtering that restricted the calls to only bi-allelic polymorphic sites, retained only
334   loci genotyped in 95% or more of all individuals, and removed loci with the fraction of
335   heterozygotes exceeding 0.6 (possible lumped paralogs), we ended up with 25,090 SNPs. In total,
336   2bRAD tags interrogated 0.18% of the genome. The genotyping accuracy was assessed based on
337   the match between genotyped replicates using script repMatchStats.pl. Overall agreement
338   between replicates was 98.7% or better with the heterozygote discovery rate (fraction of matching
339   heterozygote calls among replicates) exceeding 96%.
340
341   *Genome-wide genetic divergence*
342
343   To begin to characterize genome-wide divergence between populations we used pairwise
344   genome-wide Weir and Cockerham's F_{ST} calculated by vcftools (*38*), principal component
345   analysis (PCA) using R package adegenet (*39*), and ADMIXTURE (*40*). For PCA and
346   ADMIXTURE, the data were thinned to keep SNPs separated by 5kb on average and by at least
347   2.5 kb, choosing SNPs with highest minor allele frequency (script thinner.pl with options
348   'interval=5000 criterion=maxAF').
349
350   *Demographic analysis and bootstrapping*
351
352   Prior to demographic analysis, Bayescan (*41*) was used to identify sites potentially under
353   divergent selection among populations, and 13 such sites with q-value <0.05 were removed.
354   Demographic models were fitted to 120 bootstrapped datasets, which were generated in two
355   stages. First, five alternatively thinned datasets were generated for which SNPs were randomly
356   drawn to be on average 5 kb apart and not closer than 2.5 kb. This time the SNPs were drawn at
357   random to avoid distorting the allele frequency spectrum unlike thinning for PCA and
358   ADMIXTURE where the highest minor allele frequency SNPs were selected. Then, 20
359   bootstrapped replicates were generated for each thinned dataset by resampling contigs of the
360   reference genome with replacement (script dadiBoot.pl). The fitted model parameters were
361   summarized after excluding bootstrap replicates that fell into the lowest 15% likelihood quantile
362   and the ones where model fitting failed to converge, leading to some parameters being
363   undetermined or at infinity (less than 10% of total number of runs). Delta-AIC values were
364   calculated for each bootstrap replicate that passed these criteria for both compared models, and
365   summarized to obtain bootstrap support value, the percentage of replicates favoring the
366   alternative model. While fitting *dadi* models, the data for each population were projected to
367   sample sizes maximizing the number of segregating sites in the analysis, resulting in 7000-8172
368   segregating sites per population.
369
370   *Unit conversion*
371
372   To convert *dadi*-reported coalescent parameter values (θ, T and M) into time in years (t), effective
373   population sizes in number of individuals (Ne) and migration rates as fraction of new immigrants
374   per generation (m), we estimated the mutation rate (μ) from the time-resolved phylogeny of

10

375   *Acorpora* genus based on *paxC* intron (*42*), at 4e-9 per base per year. Although *A. millepora* was
376   shown to start reproducing in 3 years (*18*) we assumed the generation time of 5 years reasoning
377   that it would better reflect the attainment of full reproductive potential as the colony grows.
378   Assuming a genome size of 5e+8 bases (*33*) the number of new mutations per genome per
379   generation is 10. Since the fraction 2bRAD-sequenced genome in our experiment was 1.8e-3, the
380   mutation rate per 2bRAD-sequenced genome fraction per generation is $\mu = 0.018$. This value was
381   used to obtain:
382   -   Ancestral effective population size: $Ne = \theta / 2\mu$
383   -   Migration rate: $m = M / 2Ne$
384   -   Time in years: $t = 2TNe \cdot 5$
385
386   *Biophysical model*
387
388   A spatially-explicit biophysical modeling framework (*12*, *43*) was used to quantify migration
389   between coral reef habitats of the broader region surrounding the Great Barrier Reef, thereby
390   revealing the location, strength, and structure of a species' potential population connectivity. The
391   model's spatial resolution of ca. 8 km coincides with hydrodynamic data for the broader region
392   (1/12.5 degree; HYCOM+NCODA Reanalysis and Analysis product; hycom.org). Our
393   biophysical dispersal model relies on geographic data describing the seascape environment and
394   biological parameters capturing coral-specific life-histories. Coral reef habitat data are available
395   from the UNEP World Conservation Monitoring Centre (UNEP-WCMC; http://data.unep-
396   wcmc.org/datasets/1) representing a globally-consistent and up-to-date representation of coral
397   reef habitat. To capture specific inter-annual variability, two decades of hydrodynamic data were
398   used from 1992 to 2013 (*44*).
399
400   Coral-specific biological parameters for *A. millipora* included relative adult density (dependent
401   on the habitat), reproductive output, larval spawning time and periodicity (e.g., Magnetic Island
402   populations spawn a month earlier than the other GBR sites (*45*)), maximum dispersal duration,
403   pre-competency and competency periods, and larval mortality (*46*, *47*). The spatially explicit
404   dispersal simulations model the dispersal kernel (2-D surface) as a 'cloud' of larvae, allowing it
405   to be concentrated and/or dispersed as defined by the bio-physical parameters. An advection
406   transport algorithm is used for moving larvae within the flow fields (*48*).
407
408   Simulations were carried out by releasing a cloud of larvae into the model seascape at all
409   individual coral reef habitat patches and allowing the larvae to be transported downstream by the
410   currents. Ocean current velocities, turbulent diffusion, and larval behavior move the larvae
411   through the seascape at each time-step. Larval competency, behavior, density, and mortality
412   determine when and what proportion of larvae settle in habitat cells at each time step. When
413   larvae encounter habitat, the concentration of larvae settling with the habitat is recorded at that
414   time-step. From the dispersal data, we derived the coral migration matrix representing the
415   proportion of settlers to each destination patch that came from a source patch, which is analogous
416   to the source distribution matrix (*49*) and is equivalent to migration matrices derived from

11

417   population genetic analysis. It is important to note that migration matrices extracted for the field
418   sites represent the potential migration through all possible stepping-stones.
419
420   *Metapopulation adaptation model*
421
422   The model was implemented in SLiM the forward evolutionary simulator, by modifying the
423   provided recipe "Quantitative genetics and phenotypically-based fitness". The model simulates
424   Fisher-Wright populations with discreet generations. At the start of the simulation, populations
425   were established at specified population sizes and pairwise migration rates (genetic replacement
426   rates), and all QTLs in all individuals were given a mutation with the effect size drawn from a
427   normal distribution with mean zero and specified standard deviation, to create standing genetic
428   variation. The phenotype of each individual was calculated as the sum of QTL effects plus
429   random noise to simulate desired heritability. Then, fitness of each individual was calculated
430   based on the difference between the individual's phenotype (thermal optimum), temperature of
431   the environment, and the setting for phenotypic plasticity, modeled as the standard deviation of
432   the Gaussian slope of fitness decline with increasing distance between phenotype and
433   environment. Then, parents were chosen to produce the next generation according to their fitness;
434   parents for immigrant individuals are chosen from among individuals in the source population.
435   New mutations at QTLs happened at the specified rate when transitioning to the next generation
436   and the effect of a new mutation replaced the previous QTL effect.
437
438   Our code was designed for general modeling of multilocus adaptation in metapopulations and can
439   process matrices of population sizes and migration rates for an arbitrary number of populations.
440   We modeled our five populations with effective population sizes and pairwise migration rates
441   inferred by *dadi* . Within the code, it is also possible to adjust:
442
443   -   Number of QTLs and the distribution of their effect sizes. To keep the model conservative,
444   we modeled only ten QTLs with normal distribution of effect sizes with a standard deviation
445   of $0.2^{o}C$. With ten QTLs, this setting implied that at the start of simulation only about 2% of
446   corals deviated from mean thermal tolerance by more than $1.5^{o}C$ in either direction. Since
447   thermal differences between our populations exceeded $3^{o}C$, this narrow variation made local
448   adaptation rather non-trivial.
449   -   Dominance of QTLs (set to 0.5 in our simulation).
450   -   Phenotypic plasticity. We modeled three plasticity settings, 0.5, 1 and 2, which corresponded
451   to 86%, 40% and 13% fitness drop when the individual's phenotypic optimum (calculated
452   based on QTLs and heritability setting) mismatched the environment by $1^{o}C$.
453   -   Heritability (proportion of phenotypic variation explained by genetics). We examined values
454   1, 0.5, 0.25 and 1e-5, the latter to confirm that no adaptation or evolution was observed when
455   the trait was not heritable.
456   -   Mutation rate, which was set to zero because we wanted to explore only the role of standing
457   genetic variation.
458

12

459   To better model population dynamics during warming period, we implemented linear scaling of
460   the population size and immigration rates with the population's mean fitness. In this way, a
461   population declining in fitness shrinks in size and stops contributing migrants to other
462   populations.
463
464   Environmental conditions are supplied to our model as a table of values for each population in
465   every generation and can be arbitrary. Here we modeled identical thermal trends across
466   populations with population-specific offsets. During pre-adaptation period lasting 2000
467   generations, the temperature was constant on average but experienced random fluctuations
468   across generations drawn from a normal distribution with a standard deviation of 0.25°C (to
469   approximate ENSO events). The temperature was offset by $+1.6^{\circ}$C in Wilkie and Magnetic
470   populations and by -1.8°C in the Keppel population, to model differences in midsummer
471   monthly mean temperature among populations (Fig. 1). After 2000 generations a linear increase
472   at 0.05°C per generation was added to simulate warming.
473
474   All combinations of parameter settings were run ten times to ensure consistency. We found that
475   with population sizes in thousands, such as in our case, the results were very consistent among
476   independent runs. We therefore did not aggregate results over many replicated runs but show one
477   randomly chosen run for each tested parameter combination.
478

487   **Data and code availability**
488   The finalized genotyping dataset in VCF format, detailed bioinformatic walkthrough, accessory
489   formatting and plotting scripts, *dadi* scripts and the SLiM model code are available from
490   https://github.com/z0on/Adaptive-pathways-of-coral-populations-on-the-Great-Barrier-Reef. Raw
491   sequencing data has been deposited to National Center for Biotechnology Information's Short
492   Reads Archive (accession number pending).
493

References

1. A. C. Baker, P. W. Glynn, B. Riegl, Climate change and coral reef bleaching: An ecological assessment of long-term impacts, recovery trends and future outlook. *Estuar. Coast. Shelf Sci.* **80**, 435–471 (2008).

2. C. A. Logan, J. P. Dunne, C. M. Eakin, S. D. Donner, Incorporating adaptive responses into future projections of coral bleaching. *Glob. Chang. Biol.* **20**, 125–139 (2014).

3. T. P. Hughes *et al.*, Climate change, human impacts, and the resilience of coral reefs. *Science.* **301**, 929–933 (2003).

4. J. M. Pandolfi, S. R. Connolly, D. J. Marshall, A. L. Cohen, Projecting coral reef futures under global warming and ocean acidification. *Science.* **333**, 418–22 (2011).

5. G. B. B. Dixon *et al.*, Genomic determinants of coral heat tolerance across latitudes. *Science.* **348**, 1460–1462 (2015).

6. P. K. Ingvarsson, Restoration of genetic variation lost – the genetic rescue hypothesis. *Trends Ecol. Evol.* **16**, 62–63 (2001).

7. G. De'ath, K. E. Fabricius, H. Sweatman, M. Puotinen, The 27-year decline of coral cover on the Great Barrier Reef and its causes. *Proc. Natl. Acad. Sci. U. S. A.* **109**, 17995–9 (2012).

8. S. Wang, E. Meyer, J. K. McKay, M. V Matz, 2b-RAD: a simple and flexible method for genome-wide genotyping. *Nat. Methods.* **9**, 808–810 (2012).

9. M. J. H. van Oppen, V. Lukoschek, R. Berkelmans, L. M. Peplow, A. M. Jones, A population genetic assessment of coral recovery on highly disturbed reefs of the Keppel Island archipelago in the southern Great Barrier Reef. *PeerJ.* **3**, e1092 (2015).

10. M. J. H. Van Oppen, L. M. Peplow, S. Kininmonth, R. Berkelmans, Historical and contemporary factors shape the population genetic structure of the broadcast spawning coral, Acropora millepora, on the Great Barrier Reef. *Mol. Ecol.* **20**, 4899–4914 (2011).

11. R. N. Gutenkunst, R. D. Hernandez, S. H. Williamson, C. D. Bustamante, Inferring the joint demographic history of multiple populations from multidimensional SNP frequency data. *PLoS Genet.* **5**, e1000695 (2009).

12. E. A. Treml, J. Roberts, P. N. Halpin, H. P. Possingham, C. Riginos, The emergent geography of biophysical dispersal barriers across the Indo-West Pacific. *Divers. Distrib.* **21**, 465–476 (2015).

13. E. A. Treml *et al.*, Reproductive Output and Duration of the Pelagic Larval Stage Determine Seascape-Wide Connectivity of Marine Populations. *Integr. Comp. Biol.* **52**, 525–537 (2012).

14. J. Lough, A. Hobday, Observed climate change in Australian marine and freshwater environments. *Mar. Freshw. Res.* **62**, 984–999 (2011).

15. B. Charlesworth, Fundamental concepts in genetics: Effective population size and patterns of molecular evolution and variation. *Nat. Rev. Genet.* **10**, 195–205 (2009).

16. W. Renema *et al.*, Are coral reefs victims of their own past success? *Sci. Adv.* **2**, e1500850 (2016).

17. B. C. Haller, P. W. Messer, SLiM 2: Flexible, interactive forward genetic simulations. *Mol. Biol. Evol.* **34**, 230–240 (2017).

18. M. Vanessa, B. Baria, D. W. Dela Cruz, R. D. Villanueva, J. R. Guest, Spawning of three-year-old Acropora millepora corals reared from larvae in Northern Philippines. *Bull. Mar. Sci.* **88**, 61–62 (2012).

19. IPCC, *Climate Change 2007 - The Physical Science Basis. Contribution of Working Group I to the Fourth Assessment Report of the IPCC* (Cambridge University Press, New York, NY, 2007).

20. R. Berkelmans, M. J. H. van Oppen, The role of zooxanthellae in the thermal tolerance of corals: a "nugget of hope" for coral reefs in an era of climate change. *Proc. R. Soc. B-Biological Sci.* **273**, 2305–2312 (2006).

21. A. H. Baird, J. R. Guest, B. L. Willis, Systematic and biogeographical patterns in the reproductive biology of scleractinian corals. *Annu. Rev. Ecol. Evol. Syst.* **40**, 551–571 (2009).

22. K. Quigley, B. Willis, L. Bay, Heritability of the Symbiodinium community in vertically- and horizontally-transmitting broadcast spawning corals. *bioRxiv.* (2017).

23. E. J. Howells *et al.*, Coral thermal tolerance shaped by local adaptation of photosymbionts. *Nat. Clim. Chang.* **2** (2011), pp. 116–120.

24. F. P. Palstra, D. J. Fraser, Effective/census population size ratio estimation: a compendium and appraisal. *Ecol. Evol.* **2**, 2357–2365 (2012).

547 25. S. R. Palumbi, D. J. Barshis, N. Traylor-Knowles, R. A. Bay, Mechanisms of reef coral resistance to
548   future climate change. *Science*. **344**, 895–8 (2014).
549 26. E. J. Howells, R. Berkelmans, M. J. H. van Oppen, B. L. Willis, L. K. Bay, Historical thermal regimes
550   define limits to coral acclimatization. *Ecology*. **94**, 1078–1088 (2013).
551 27. D. Nettle, M. Bateson, Adaptive developmental plasticity: what is it, how can we recognize it and when
552   can it evolve? *Proc. R. Soc. B Biol. Sci.* **282**, 20151005 (2015).
553 28. Great Barrier Reef Marine Park Authority, *Interim report on the environmental impacts of the 2016
554   coral bleaching event*.
555 29. T. J. Done, Phase shifts in coral reef communities and their ecological significance. *Hydrobiologia*. **247**,
556   121–132 (1992).
557 30. O. Hoegh-Guldberg *et al.*, Assisted colonization and rapid climate change. *Science*. **321**, 345–346
558   (2008).
559 31. S. N. Aitken, M. C. Whitlock, Assisted Gene Flow to Facilitate Local Adaptation to Climate Change.
560   *Annu. Rev. Ecol. Evol. Syst.* **44**, 367–388 (2013).
561 32. G. B. Dixon, L. K. Bay, M. V. Matz, Bimodal signatures of germline methylation are linked with gene
562   expression plasticity in the coral Acropora millepora. *BMC Genomics*. **15**, 1109 (2014).
563 33. C. Shinzato *et al.*, Using the Acropora digitifera genome to understand coral responses to environmental
564   change. *Nature*. **476**, 320-U82 (2011).
565 34. M. J. H. van Oppen, B. J. McDonald, B. Willis, D. J. Miller, The Evolutionary History of the Coral
566   Genus Acropora (Scleractinia, Cnidaria) Based on a Mitochondrial and a Nuclear Marker: Reticulation,
567   Incomplete Lineage Sorting, or Morphological Convergence? *Mol. Biol. Evol.* **18**, 1315–1329 (2001).
568 35. B. F. Voight, S. Kudaravalli, X. Wen, J. K. Pritchard, A map of recent positive selection in the human
569   genome. *PLoS Biol.* **4**, e72 (2006).
570 36. I. K. Jordan *et al.*, A universal trend of amino acid gain and loss in protein evolution. *Nature*. **433**, 633–
571   8 (2005).
572 37. A. Mckenna *et al.*, The Genome Analysis Toolkit: A MapReduce framework for analyzing next-
573   generation DNA sequencing data. *Genome Res.* **20**, 1297–1303 (2010).
574 38. P. Danecek *et al.*, The variant call format and VCFtools. *Bioinformatics*. **27**, 2156–8 (2011).
575 39. T. Jombart, adegenet: a R package for the multivariate analysis of genetic markers. *Bioinformatics*. **24**,
576   1403–5 (2008).
577 40. D. H. Alexander, J. Novembre, K. Lange, Fast model-based estimation of ancestry in unrelated
578   individuals. *Genome Res.* **19**, 1655–64 (2009).
579 41. T. Günther, G. Coop, Robust identification of local adaptation from allele frequencies. *Genetics*. **195**,
580   205–20 (2013).
581 42. Z. T. Richards, D. J. Miller, C. C. Wallace, Molecular phylogenetics of geographically restricted
582   Acropora species: Implications for threatened species conservation. *Mol. Phylogenet. Evol.* **69**, 837–851
583   (2013).
584 43. E. A. Treml, P. N. Halpin, D. L. Urban, L. F. Pratson, Modeling population connectivity by ocean
585   currents, a graph-theoretic approach for marine conservation. *Landsc. Ecol.* **23**, 19–36 (2008).
586 44. E. P. Chassignet *et al.*, The HYCOM (HYbrid Coordinate Ocean Model) data assimilative system. *J.
587   Mar. Syst.* **65**, 60–83 (2007).
588 45. R. C. Babcock *et al.*, Synchronous Spawnings of 105 Scleractinian Coral Species on the Great-Barrier-
589   Reef. *Mar. Biol.* **90**, 379–394 (1986).
590 46. S. W. Davies, E. A. Treml, C. D. Kenkel, M. V. Matz, Exploring the role of Micronesian islands in the
591   maintenance of coral genetic diversity in the Pacific Ocean. *Mol. Ecol.* **24**, 70–82 (2015).
592 47. S. R. Connolly, A. H. Baird, Estimating dispersal potential for marine larvae: dynamic models applied
593   to scleractinian corals. *Ecology*. **91**, 3572–3583 (2010).
594 48. P. K. Smolarkiewicz, J. Szmelter, An MPDATA-based solver for compressible flows. *Int. J. Numer.
595   Methods Fluids*. **56**, 1529–1534 (2008).
596 49. R. K. Cowen, G. Gawarkiewicz, J. Pineda, S. Thorrold, F. Werner, Population Connectivity in Marine
597   Systems: An Overview. *Oceanography*. **20**, 14–21 (2007).
598

15

599 **Supplemental Figures**
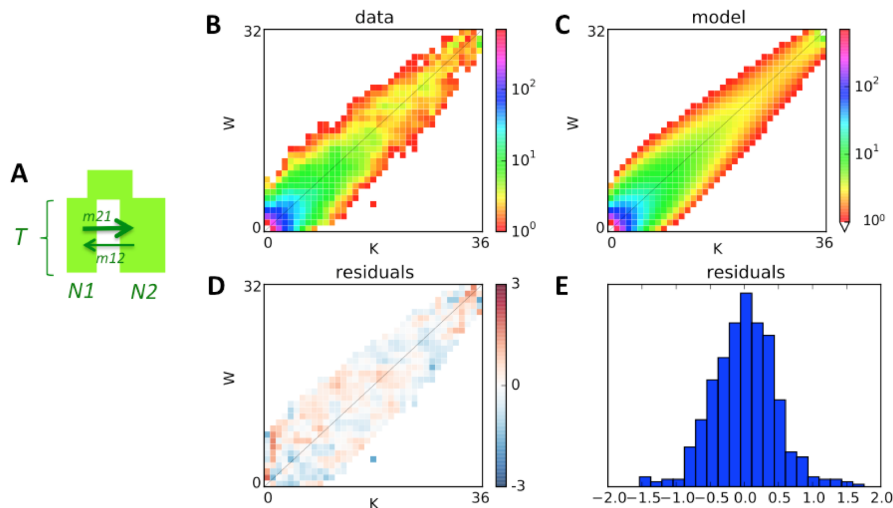600
601
602
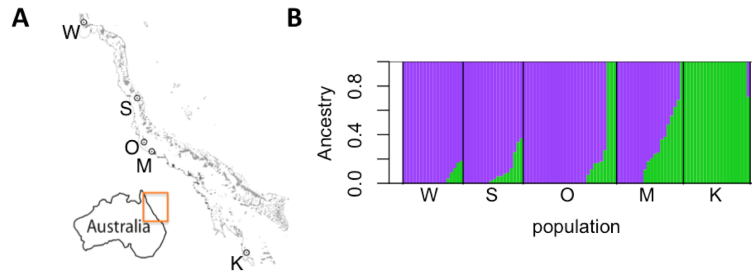
603
604   Figure S1. ADMIXTURE analysis of genetic differentiation between populations. (A) Map of sampled
605   locations with one-letter population identifiers. (B) ADMIXTURE plot of ancestry proportions with $K = 2$
606   (optimal K was 1).
607
608
609
610
611

612
613   Figure S2. Example of two-population *dadi* model fit. (A) The model: ancestral population splits into two
614   populations of unequal sizes (N1 and N2) some time T in the past, which exchange migrants with different
615   rates depending on direction. (B) Observed allele frequency spectrum comparing Wilkie (W) and Keppel
616   (K) populations. (C) Allele frequency spectrum generated by the fitted model. (D, E) Map and histogram of
617   residuals (absolute scale).
618

16

619
620
621
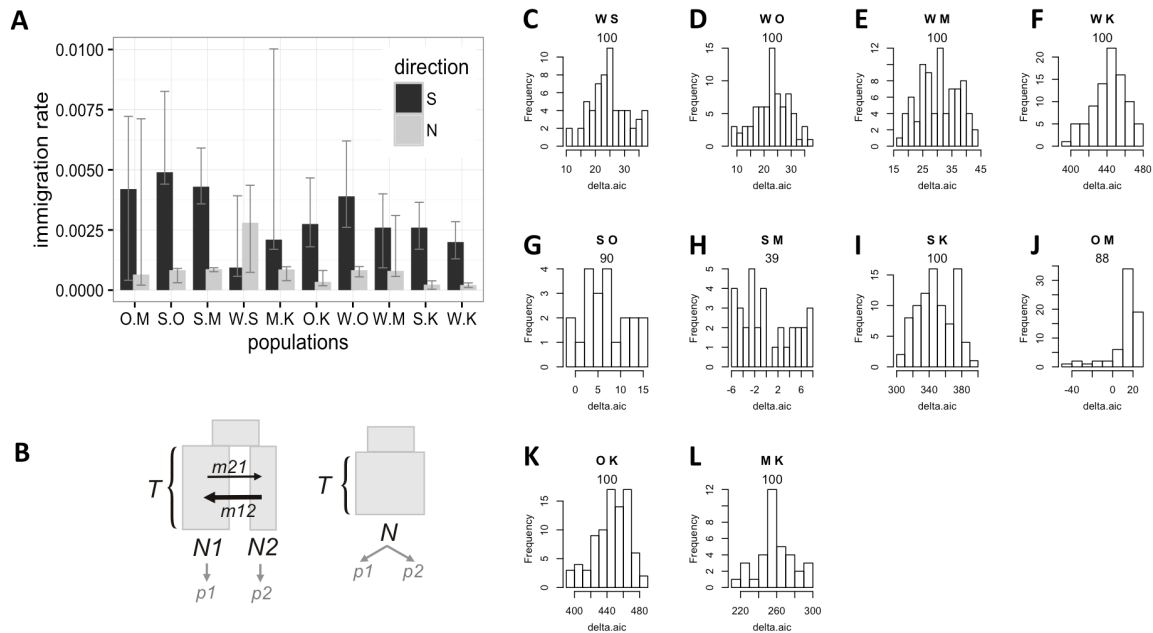
622
623 Figure S3. Bootstrap analysis of migration rates and population subdivision using *dadi*. (A) Migration
624 among population pairs, with bootstrap-derived 95% confidence intervals. The pairs are identified on the x-
625 axis and sorted by increasing geographical distance. Black bars – southward migration, grey bars –
626 northward migration. (B) Models being compared: the full model (left) implies populations' split into two
627 different sizes (N1 and N2) at time T in the past, since when they exchanged migrants at unequal rates
628 depending on direction. Reduced model allows for population size change at time T in the past but does not
629 include population split: the two genotyped groups (p1 and p2) are regarded as two samples from the same
630 population. (C-L) Histograms of delta-AIC values for 100 bootstrap replicates (bootstrap was performed
631 over genomic contigs of the draft genome of *A. digitifera*. Positive numbers indicate support for the full
632 model. The letters on top of each panel identify compared populations, the number is the proportion of
633 positive bootstrap replicates (i.e., bootstrap support for the full model). The only comparison that did not
634 receive >50% bootstrap support for population split is between S and M populations (panel H).
635

636
637
638
639
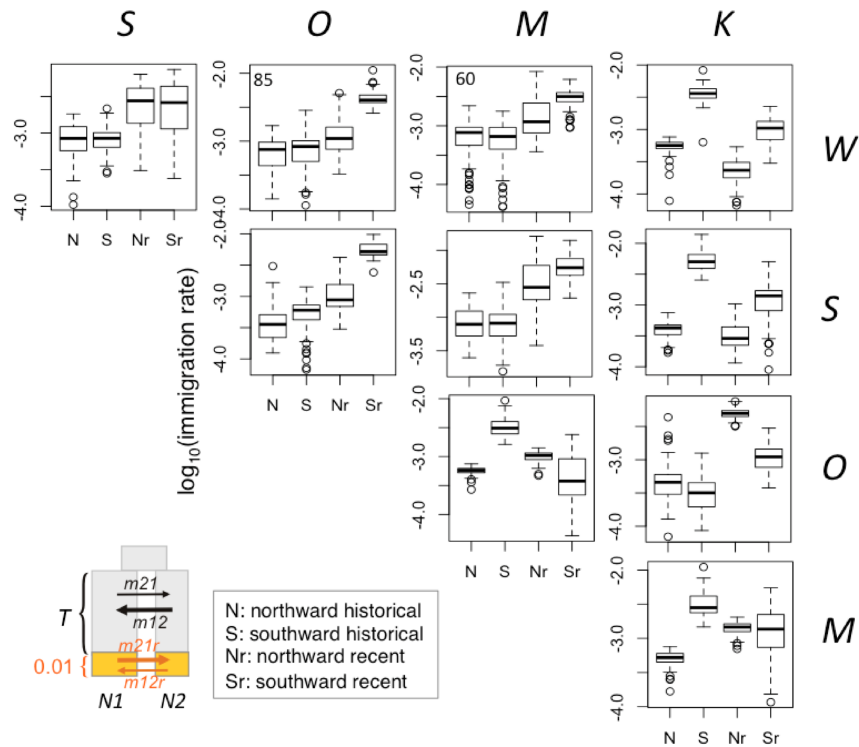
640
641 Figure S4. Migration rates inferred by the *dadi* model allowing for the change in migration rates over the
642   last 0.01 T units (15-20 generations or 75-100 years, in our case). Box plots show historical (N, S) and
643 recent (Nr, Sr) migration rates inferred among pairs of population across 100 bootstrap replicates. Numbers
644   in the top left corner of the WO and WM plots are delta-AIC bootstrap support values for the model with
645   the recent change in migration when compared to the split-with-migration model with no recent change
646   (Fig. 1A). All other pairs had less than 50% delta-AIC bootstrap support. There is no consistent recent
647   change in the preferential direction of migration.

648
649
650
651
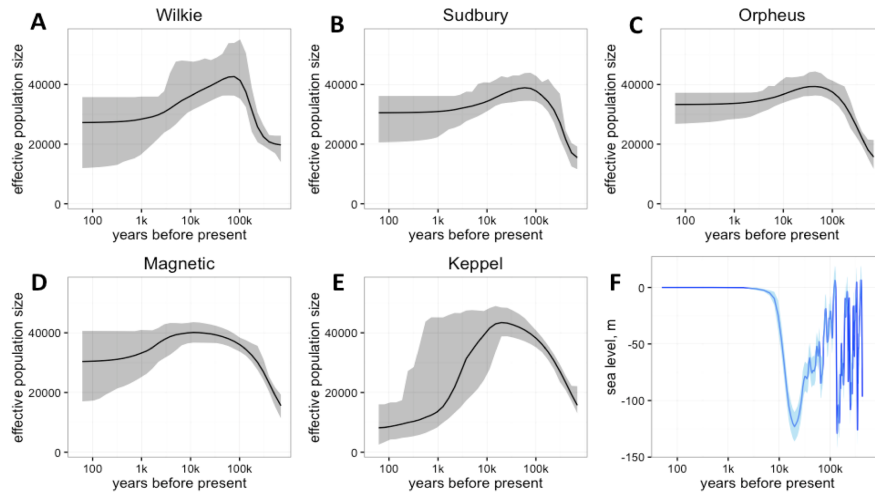
652
653   Figure S5. Population history. (A-E) Historical population sizes with bootstrap-derived 95% confidence
654   intervals, according to the two-growth model (Fig. S6 A). (F) Sea level with shaded area corresponding to
655   standard error (*41*).
656
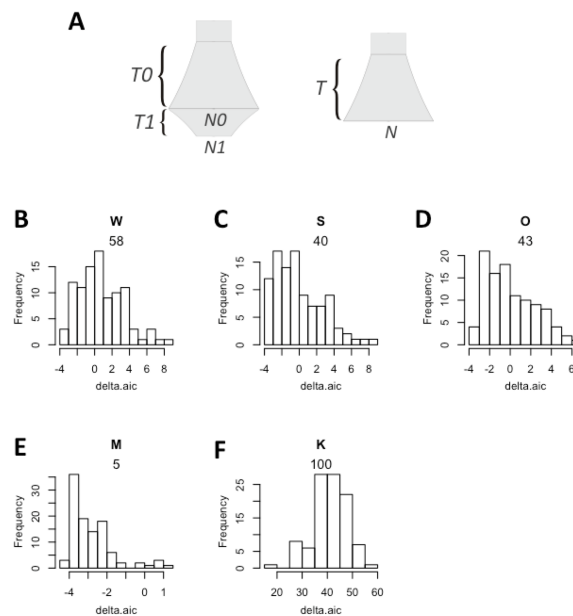
657
658   Figure S6. Delta-AIC bootstrap analysis of single-population models. (A) Models compared. The full
659   model (left) includes two exponential growth periods (any of which could be growth or decline), the
660   reduced model (right) has only one growth period. (B-F) Histograms of delta-AIC values for 100 bootstrap
661   replicates. Positive numbers indicate support for the full model. The letter on top of each panel identify the
662   population, the number is the proportion of positive bootstrap replicates (i.e., bootstrap support for the full
663   model). The two-growth model is strongly supported for population K (panel F) and marginally supported
664   for population W (panel B).
665
666

19
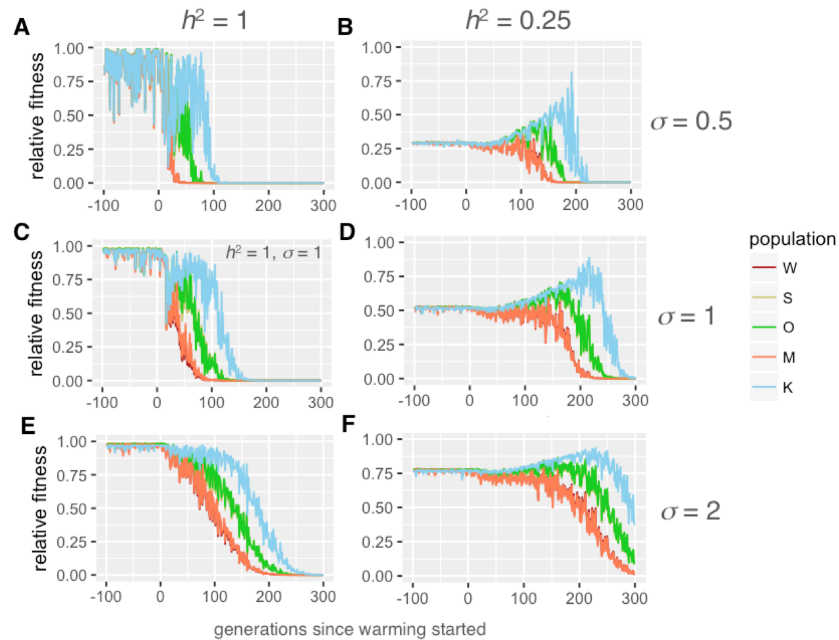
667
668   Figure S7. Fitness of modeled populations after pre-adaptation period and under warming, depending on
669   heritability of thermal tolerance (h^2, proportion of phenotypic variation explained by genetics) and
670   phenotypic plasticity (σ, standard deviation of the Gaussian slope of fitness decline away from the
671   phenotypic optimum, in degrees C). X-axis is generations; warming starts at generation 0. Y-axis is fitness
672   relative to maximal fitness at the genetically determined optimum. Warm-adapted populations (W and M)
673   are shown as red-tint traces, populations from mild thermal regime (S and O) are green-tint traces, and the
674   cool-adapted population (K) is the blue trace. Pairs of traces for warm- and mild-adapted populations
675   largely overlap. (A, C, E): h^2=1. (B, D, F): h^2=0.25. (A, B): σ = 0.5. (C, D): σ = 1. (E, F): σ = 2. Higher
676   plasticity facilitates metapopulation persistence during warming and confers stability against random
677   fluctuations. Higher plasticity also partially rescues the drop in fitness achievable under low heritability
678   (compare pre-warming generations, from -100 to 0, on panels B, D and F).
679

680
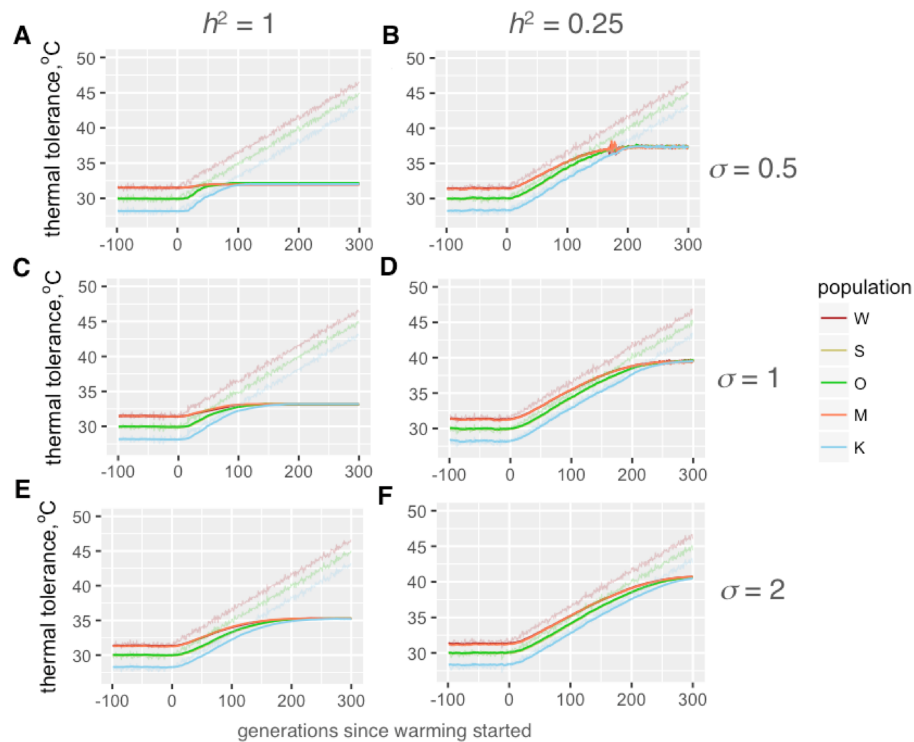
681
682 Figure S8. Higher plasticity and lower heritability promote longer and more extensive evolution in response
683   to warming. The graphs show mean thermal tolerance of modeled populations after pre-adaptation period
684   and under warming, depending on heritability of thermal tolerance (h^2, proportion of phenotypic variation
685   explained by genetics) and phenotypic plasticity (σ, standard deviation of the Gaussian slope of fitness
686   decline away from the phenotypic optimum, in degrees C). X-axis is generations; warming starts at
687   generation 0. Y-axis is thermal tolerance (mean phenotype of the population). Warm-adapted populations
688   (W and M) are shown as red-tint traces, populations from mild thermal regime (S and O) are green-tint
689   traces, and the cool-adapted population (K) is the blue trace. Thin noisy lines are modeled temperatures at
690   the corresponding locations. Pairs of traces for warm- and mild-adapted populations largely overlap. (A, C,
691   E): h^2=1. (B, D, F): h^2=0.25. (A, B): σ = 0.5. (C, D): σ = 1. (E, F): σ = 2.
692
693

21
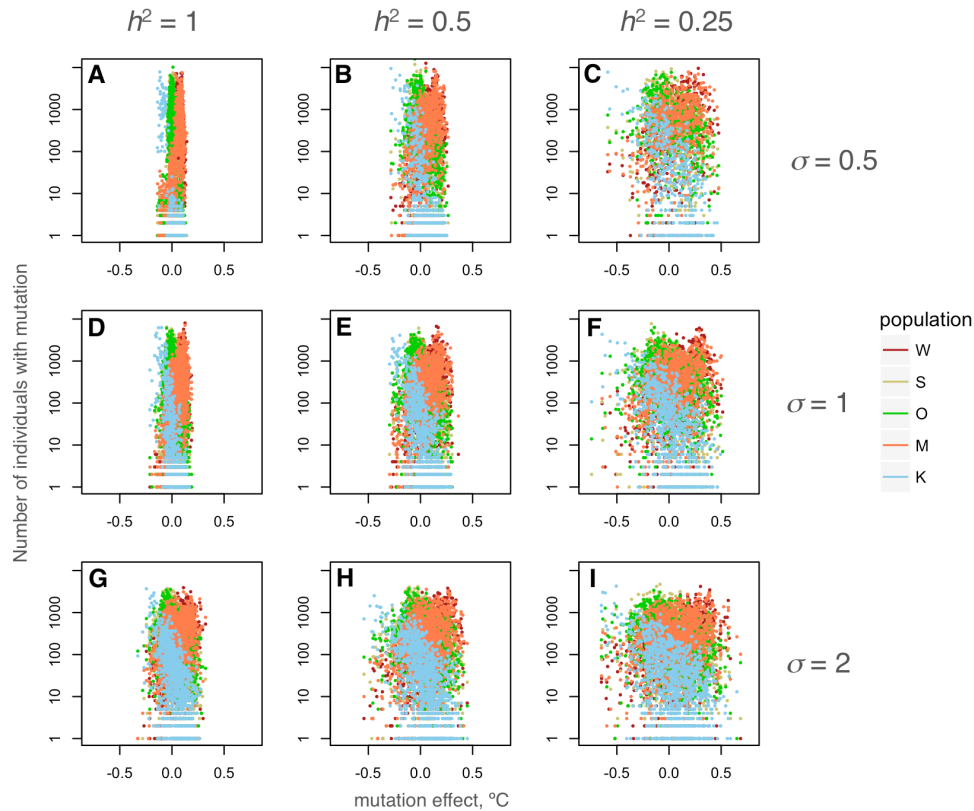
694
695
696   Figure S9. Higher plasticity (σ) and lower heritability (h^2) promote retention of higher genetic variation in
697   thermal tolerance. The scatterplots show the dependence of the number of individuals in a population
698   bearing a mutation at a thermal QTL locus on the mutation's effect size (change in thermal tolerance, in ºC)
699   at the end of the pre-adaptation period (2000 generations with no directional change in temperature). The
700   starting standing genetic variation was the same in all simulations. (A,D,E): h^2=1. (B,E,H): h^2=0.5. (C,F,I):
701   h^2=0.25. (A-C): σ = 0.5. (D-F): σ = 1. (G-I): σ = 2. Populations are colored according to the color scheme
702   used in Figures 3, S7 and S8 (see legend).
703

22